GEDI Elevation Accuracy Assessment: A Case Study of Southwest Spain

Elia Quirós, María-Eugenia Polo, and Laura Fragoso-Campón

***Abstract*—Information about forest structures is becoming crucial to earth's global carbon cycle, forest habitats, and biodiversity. The Global Ecosystem Dynamics Investigation (GEDI) provides 25-m diameter footprints of the surface for 3-D structure measurements. The main goal of this study is to compare 12 031 footprints of GEDI data with other airborne and spaceborne digital elevation models (DEMs) for Southwest Spain. Ground elevation differences [elevation of the lowest mode (ELM)] are analyzed by comparing GEDI measurements with airborne laser scanning (ALS) LiDAR- and TanDEM-X-derived DEMs. The vertical structure (RH100) is compared to the ALS LiDAR measurement. Ten zones are analyzed, considering different degrees of coverage and slopes. We achieved a root mean square error (RMSE) of 6.13 m for the ELM when comparing GEDI and LiDAR data and an RMSE of 7.14 m when comparing GEDI and TanDEM-X data. For some of the studied areas, these values were considerably smaller, with RMSE values even lower than 1 m. For the RH100 metric, an RMSE of 3.56 m was achieved when comparing GEDI and LiDAR data, but again with a minimum value of 2.09 m for one zone. The results show a clear relation to coverage and slope, especially for the latter. This work also evaluates the positional uncertainty of GEDI footprints, shifting them ± 10 and ± 5 m along and across the track of the satellite orbit and their intermediate angular positions. The outcomes reveal a strong tendency to obtain better results in the ELM when setting the footprint to 270° and displacing it within 10 m of its positional uncertainty in comparison with the LiDAR and TanDEM-X data.**

***Index Terms*—Digital elevation models (DEMs), error analysis, forestry, uncertainty, vegetation mapping.**

I. Introduction

In RECENT years, LiDAR technology has become a powerful tool for the study of the earth's surface from a 3-D perspective. LiDAR remote sensing from three platforms—ground, airborne, and spaceborne—has the potential to acquire direct 3-D measurements of the forest canopy that are useful for estimating a variety of forest inventory parameters [1].

Manuscript received November 11, 2020; revised February 16, 2021; accepted May 12, 2021. Date of publication May 17, 2021; date of current version June 4, 2021. This work was supported in part by the Consejería de Economía, Ciencia y Agenda Digital of Junta de Extremadura (Spain) and co-funded by the European Regional Development Fund under Grant GR18028 (KRAKEN) and Grant GR18052 (DESOSTE). The work of Laura Fragoso-Campón was supported by the Consejería de Economía, Ciencia y Agenda Digital of Junta de Extremadura and the European Social Fund under Grant PD16018. *(Corresponding author: Elia Quirós.)*

Elia Quirós and Laura Fragoso-Campón are with the Department of Graphic Expression, University of Extremadura, Polytechnic School, 10003 Cáceres, Spain (e-mail: equiros@unex.es; laurafragoso@unex.es).

María-Eugenia Polo is with the Department of Graphic Expression, University of Extremadura, University Centre of Mérida, 06800 Mérida, Spain (e-mail: mepolo@unex.es).

Digital Object Identifier 10.1109/JSTARS.2021.3080711

Airborne laser scanning (ALS) has been, in recent decades, the main source of information used for forest structure modeling. Large areas or even whole countries are covered with 3-D point clouds collected by ALS systems [2]. ALS data are used in multiple forest settings, such as to estimate aboveground biomass [3], to determine forest fuel characteristics of mortality-affected forests [4], to delineate crowns and classify tree species [5]–[7], or even to separate overstories and understories in forested areas [8], in some cases in combination with spectral images.

Two spaceborne laser scanners with the ability to scan vegetation structures, the ICEsat-2 and Global Ecosystem Dynamics Investigation (GEDI) missions, were launched in 2018. In the case of ICEsat-2, this was not its main objective, as its central mission was to enable the estimation of heights of ice sheets and sea ice thickness. However, it can provide an initial estimation of global vegetation height [9]. From its launch, it has been used to estimate aboveground biomass and forest canopy cover in Narine *et al.* [10] and even to map forest canopy height in Li *et al.* [11] with other satellite images.

On December 5, 2018, the National Aeronautics and Space Administration (NASA) launched the GEDI spaceborne LiDAR sensor, designed to measure the earth surface structure and canopy structure of vegetation and to provide a biomass map at a 1 km spatial resolution [12]. The GEDI was deployed on the International Space Station (ISS) and started operations on March 25, 2019. The GEDI mission, which is scheduled to be operational for at least two years, is expected to collect approximately 10 billion cloud-free land surface observations. The goal of the GEDI mission is to provide data for studying forest structures and biomass in tropical and temperate environments of between 51.6° north and south, following the ISS path and being the first instrument specifically optimized to measure vegetation structures [13].

The GEDI instrument is comprised of three geodetic-class lasers, one of which is split into two weaker energy beams, resulting in four GEDI beams that are optically dithered to form eight parallel tracks. These parallel tracks are spaced 600 m across the flight track direction, leaving a distance of 4.2 km between the first and last tracks. Each laser shoots 242 times per second, creating a footprint with a 25 m diameter on the surface on which the 3-D structure is measured. The edge of every footprint is separated 35 m from the following or, equivalently, the footprint centers are separated 60 m apart [13], [14].

The GEDI provides some data products for each footprint that can be freely downloaded from the NASA EarthData Platform.[1]

[1]Online. [Available]: https://earthdata.nasa.gov/

There are several levels of products available for download [13]. The raw waveforms collected by the system are delivered at the L1A level. Waveforms processed to identify ground elevation, canopy top height, and relative height (RH metrics) are included in the L2A dataset. In L2B, various canopy metrics are calculated. Level 3 products are gridded by spatially interpolating L2 footprint estimates of topography, canopy height, canopy cover, the leaf area index (LAI), vertical foliage profiles and their uncertainties. Level 4 products are the highest levels GEDI products, and they measure above-ground biomass density. Level 1B, Level 2A, and Level 2B data from the GEDI are available from the Land Processes DAAC.[2] Gridded Level 3 GEDI data will be available from ORNL DAAC beginning in mid-2020 with Level 4 data to follow in early 2021.

GEDI data are being used for multiple purposes, such as to estimate time since the last stand-replacing disturbance to model forest ecosystem processes [15], estimate biomass [14], [16], estimate forest height [17], explore the relation between the vertical canopy structures and tree species [18], detect changes in forest structures [19], map the diversity of canopy structures [12], or even define the elevation for inland waterbody altimetry [20].

LiDAR systems are not the only systems with the ability to provide 3-D information about the surface of the earth. Synthetic aperture radar (SAR) has been used for forest monitoring for several years. SAR satellites have been proven to discriminate forest/vegetation [21], [22], not only to map forest vegetation [23]–[25] but also to characterize the vertical forest structure [26] to estimate forest aboveground biomass [27]–[29] and many other variables.

Several SAR satellites can be used for forest monitoring [30], such as SENTINEL 1 [31], ALOS PALSAR [32], ICESat GLAS [11], ENVISAT ASAR and RADARSAT [33], and one of the most used, TanDEM-X (TDX) [34]. Since September 2010, a second satellite TDX was added to TerraSAR-X for the acquisition of a global digital elevation model (DEM) from bistatic X-band interferometric SAR acquisitions. The TDX mission was financed by a public-private partnership between DLR and Airbus Defense and Space. Since September 2016, the TDX DEM has been considered one of the most consistent, highly accurate, and complete global DEM datasets of the earth's surface [35]. There are several DEM products: the TDX DEM, the TDX Intermediate DEM, and DEMs for special user requests. The first is a global product with a nominal pixel of 0.4 arcseconds that corresponds to approximately 12 m. The DEM's production includes the generation of other information layers, such as height error map data, which represent the height error [standard deviation (SD)], from rigorous error propagation. Many studies have confirmed the usefulness of the TDX DEM for various purposes. It is used mainly for flood detection [36] and other hydrological purposes [37]. However, works have also used the model to obtain canopy height models for forested areas [38].

As noted earlier, GEDI measurements of forest canopy height, canopy vertical structures, and surface elevation are used to characterize important carbon and water cycling processes, biodiversity levels, and habitats [39], but as the GEDI is a sampling mission, it is limited in the spatial resolution of grids (wall-to-wall) that can be produced. A finer, continuous spatial resolution can be achieved by combining these data with other remote sensing data [13], [40]. The fusion approach from GEDI and TDX indicates a great possibility for generating global-scale forest maps and biomass maps (where the GEDI data will be available) with unprecedented spatial resolution [41]. In this sense, GEDI data are combined with TDX measurements in Choi *et al.* [42], Lee *et al.* [41], and Lee *et al.* [43] to express physical forest structure. This approach was also used for forest structure modeling before the GEDI launch [44] with simulated GEDI data.

Additionally, GEDI data have been combined with ALS, but in this case, this was not done to extrapolate the intermittent GEDI measurements but to evaluate the accuracy of both datasets, especially in quantifying the biomass and vertical structure of vegetation. The assessment of GEDI and ALS measurements has been carefully analyzed in Silva *et al.* [45] and Hancock *et al.* [46] but with simulated GEDI observations. It is challenging to interpolate the data between spotted data to match with the other optical images (continuous overage data). To prove the method and validate the height data, the ground locations between field measurement places and laser shot area have to be matched accurately [47].

Therefore, the study of differences in elevation between actual data captured by the GEDI satellite and other sources of information with which it is usually combined is now necessary. The GEDI is proving to spur a major revolution in global forest monitoring. As stated in Duncanson *et al.* [14], the accuracy of vegetation metrics depends on the accuracy of the ground elevation estimation for each waveform. Its recent emergence means that its accuracy, in terms of measured elevations (terrain height and canopy height), has not been studied in detail, and it is necessary, while the GEDI mission's ground finding algorithm is still under development [14].

In this way, the overall goal of this study is to compare GEDI elevation real data with other airborne and spaceborne DEM data for Southwest Spain. For this purpose, ground elevation differences were analyzed by comparing GEDI measurements with ALS- and TDX-derived DEMs. Complementarily, and due to the great importance of vertical structure data for the GEDI sensor, differences between vegetation heights and the elevations of its upper end were compared to ALS measurements. Finally, all comparisons have been extended to the whole area of uncertainty in geolocation of the footprint, studying whether there is any predominant trend for a better fit between GEDI measurements and ALS- and TDX-derived DEMs.

II. Study Area and Datasets

The study areas are located in Southwest Spain in the region of Extremadura of the province of Cáceres, which extends across latitudes of 39.03° to 40.48° N and longitudes of 7.54° to 4.95° W. The climatic characteristics of the study area correspond to the Mediterranean pluviseasonal continental variant [48] (see Fig. 1). Ten zones with varied vegetation cover, different elevations, and diverse relief characteristics were chosen (see Table I).

[2]Online. [Available]: https://daac.ornl.gov/cgi-bin/dataset_lister.pl?p=40

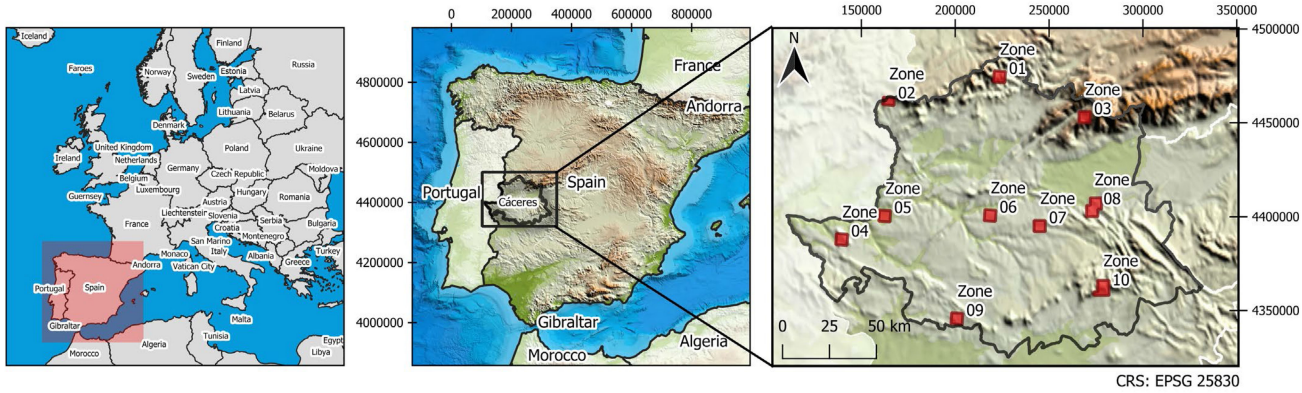

Fig. 1. Study area divided into ten zones.

TABLE I
GENERAL CHARACTERISTICS OF EACH ZONE

Zone	Mean Elevation (m)	Mean Slope (º)	Predominant Coverage	Mean Percentage of Cover (%)
Zone 01	918	25.4	Mixed forest	35.0
Zone 02	766	18.1	Coniferous forest	41.7
Zone 03	1 397	22.6	Sclerophyllous vegetation	10.1
Zone 04	466	12.2	Sclerophyllous vegetation	26.0
Zone 05	286	13.3	Natural grassland	10.25
Zone 06	438	3.4	Agroforestry areas	4.6
Zone 07	449	6.8	Agroforestry areas	14.7
Zone 08	444	15.0	Agroforestry areas	22.2
Zone 09	484	9.3	Agroforestry areas	24.9
Zone 10	816	15.9	Broad-leaved forest	24.7

Three different datasets were used in this study: the GEDI dataset, which is the target dataset to be studied in terms of accuracy, the TDX dataset, which is our first source of comparative data, and the ALS LiDAR dataset, which is our second source of comparative data and, in terms of accuracy and temporal acquisition closeness, our most robust source of comparison.

GEDI is expected to obtain canopy heights generally accurate to about 1 m [49], [50]. Based on the prelaunch assessment and assuming full system calibration, the geolocation uncertainty of the data is 10 m [49]. Data were captured between May and September 2019.

The TDX DEM has an absolute horizontal and vertical accuracy level of 10 m in general. For slopes of less than 20%, the relative vertical accuracy is 2 m, and for slopes of greater than 20%, this relative accuracy is 4 m [35]. Data were acquired between 2011 and 2014.

LiDAR data were acquired between late 2018 and early 2019 with a resolution of 2 points/m^2. In terms of accuracy, LiDAR data have an altimetric root mean square error (RMSE) of 0.15 m and planimetric RMSE of 0.30 m [51]. These features make these data the most accurate source used in this work.

The altimetric heights of the three data sources refer to the WGS-84 ellipsoid.

III. METHODOLOGY

A. Data Preparation

1) GEDI Data: GEDI data products are recorded for the full ISS orbits and are available for download at three levels of processing: Level 1B Geolocated Waveform Data, Level 2A Elevation and Height Metrics Data, and Level 2B Canopy Cover and Vertical Profile Metrics Data. We used the GEDI Finder service to identify orbits over the study area. Then, the GEDI data were processed with the rGEDI R package [52].

First, we read the data for the full orbit and clipped within the boundary box of the Extremadura region. Second, the elevation and height metrics were extracted from GEDI Level 2A data for the selected footprints within the study area. The following GEDI information was extracted (see Fig. 2).

1) The *shot number*, which corresponds with the unique footprint identifier of every footprint in the orbit.
2) *Degrade flags* indicating the degraded state of pointing and/or positioning information and showing a potential issue with the data.
3) *Quality flags*, which indicate whether the waveform data are likely to be valid (1) or invalid (0).
4) The elevation of the highest return (EHR) corresponding to the elevation of the highest detected return relative to reference ellipsoid.
5) The elevation of the lowest mode (ELM) corresponding to the elevation of the center of the lowest mode of the received waveform in the footprint.
6) *RH100* corresponding to the relative height metrics of the highest detected return (100%) and representing the difference in elevation between the highest detected return and mean ground elevation in the footprint.

The data were filtered, discarding all footprints with degraded or invalid quality flags (0), and finally, the spatial position of the footprints was exported to shapefile format for their analysis in GIS software. As a result, a total of 12 031 footprints were used.

2) LiDAR Data: LiDAR data were processed with FUSION software [53], a primary research tool.

The first operation involved extracting the ground level. GroundFilter tool is designed to filter a cloud of LiDAR returns to identify returns that lie on the probable ground surface

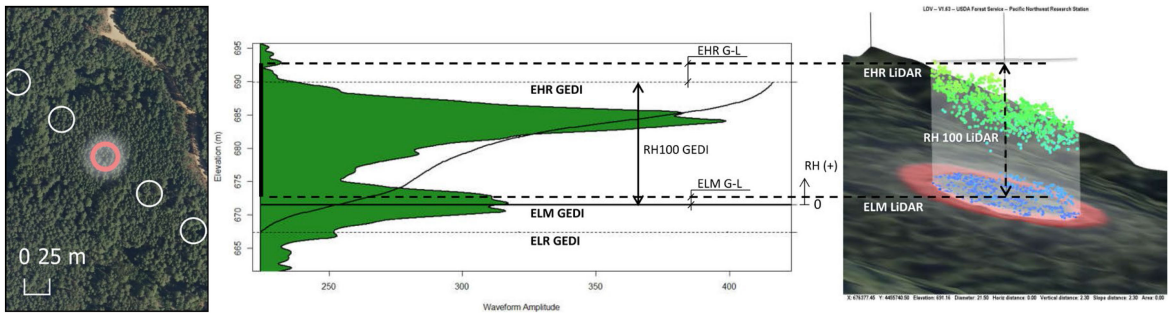

Fig 2. Interpretation of GEDI RH Metrics.

(bare-earth points) [54]. This algorithm is based on linear prediction and is implemented as an iterative process where some parameters need to be set. In the first step, a surface is computed with equal weights for all LiDAR points. This creates a surface that lies between the true ground and the canopy surface. Terrain points are more likely to be positioned below the surface while vegetation points are more likely to be positioned above the surface. The distance and direction to the surface are used to compute weights for each LiDAR point using the following weight function [54]:

$$P_i = \begin{cases} 1 & \text{If } v_i \leq g \\ \frac{1}{1+(a(v_i-g)^b)} & \text{If } g \leq V_i \leq g+w \\ 0 & \text{If } g+w < v_i \end{cases} \quad (1)$$

Parameters a and b determine the steepness of the weight function. The shift value, g, determines, which points are assigned the maximum weight value of 1.0. The above ground offset parameter, w, is used to establish an upper limit for points to have an effect on the intermediate surface. In this study, values of $a = 1, b = 4, g = -1$, and $w = 1.25$ were set. This combination is the one that works best for LiDAR low-density point resolution.

After the final iteration, bare-earth points are selected using the final intermediate surface. All points with elevations that satisfy the first two conditions of the weight function are considered bare-earth points [54].

The filtered bare earth point cloud was used to generate a DEM using the GridSurfaceCreate tool, which computes cell elevations using the average elevation of all points within a cell. Additionally, a digital surface model (DSM) was created to represent canopy cover using the CanopyModel tool, which creates a canopy surface model using the LiDAR point cloud and assigns to each pixel the EHR. A spatial resolution of 2 m was used for the DEM and DSM.

Additionally, a cover analysis was performed by means of the Cover tool. Cover computes estimates of canopy closure using a grid. Output values for cover estimates range from 0.0% to 100.0%. Canopy closure is defined as the number of returns over a specified height threshold divided by the total number of returns within each pixel [54]. In this study, this height threshold was set at 1 m aboveground. The spatial resolution was also set to 2 m to generate this cover raster.

3) TDX Data: TDX DEM data did not need further preparation. The DEM contains the final global digital elevation of the land masses of the earth. It predominantly represents a DSM. Elevated objects are included, but heights might be affected by inherent SAR effects.

B. Height Extractions

Once all rasters were prepared, the heights were calculated within all GEDI footprints.

To draw a good comparison, heights were extracted following the same references of GEDI data. Thus, the most important metrics derived from GEDI measurements are as follows (see Fig. 2).

1) The ELM: The mean ground elevation in the footprint.
2) The EHR: The highest detected return in the footprint.
3) RH100: The difference in elevation between the highest detected return and the mean ground elevation in the footprint.

Following these metrics, the mean ground elevation in the footprint was calculated for the LiDAR DEM and TDX DEM in all zones. Additionally, the highest detected return was obtained for the LiDAR DSM. With the LiDAR extracted elevations, the RH100 metric (difference in elevation between the highest detected return and mean ground elevation) was also obtained for the LiDAR datasets.

C. Statistical Analysis

1) Global Statistics: As previously defined, the heights used are called the ELM, EHR, and RH100. The mentioned heights together with the three available sources of data used in this study (GEDI, LiDAR, and TDX DEM) generate the following seven heights:

1) ELM GEDI;
2) ELM LiDAR;
3) ELM TDX;
4) EHR GEDI;
5) EHR LiDAR;
6) RH100 GEDI;
7) RH100 LiDAR.

From these variables, the following differences in heights were calculated, with their analysis being the focus of this article.

1) ELM G-L: The difference in the mean ground elevation in the footprint between GEDI and LiDAR data.
2) ELM G-T: The difference in the mean ground elevation in the footprint between GEDI and TDX data.
3) EHR G-L: The difference in the highest detected return in the footprint between GEDI and LiDAR data.

TABLE II
NUMBER OF FOOTPRINTS IN EACH ZONE

Zone	Footprints	Zone	Footprints
Zone 01	1073	Zone 06	189
Zone 02	903	Zone 07	964
Zone 03	676	Zone 08	1672
Zone 04	2108	Zone 09	769
Zone 05	1237	Zone 10	2440

4) RH100 G-L: The difference in elevation between the highest detected return and mean ground elevation in the footprint between GEDI and LiDAR data.

It should be noted that any observation classified as an outlier has been discarded using the interquartile range (IQR) criterion for RH100 LiDAR values, where some anomalous values were observed. This criterion means that all observations above third quartile $+1.5 \cdot$IQR are considered outlier values.

The statistical analysis was performed using R software [55]. First, the full set of 12 031 heights and differences in heights were analyzed to determine the behavior of both the heights and the differences. The statistical analyses involved the calculation of the mean value, SD, mean standard error (MSE), median, maximum, and minimum values, interquartile rank (IQR) and coefficients of skewness and kurtosis. The RMSE for the differences in the heights was also calculated, for GEDI-LiDAR differences in the ELM.

Box plots were drawn to graphically compare both the heights and the differences in heights. A scatterplot showing the correlation between each height and difference in heights with the terrain slope and the level of cover was plotted, and the correlation index for each case was also calculated.

A scale of slope ranges was established to identify a correlation between the heights and differences in heights and the slope of the terrain. The scale of terrain slopes measures at intervals of 5 over 5 units, with the first category referring to values of between 0 and 5, called "ts_00-05," and with the last pertaining to values of greater than 40, called "ts_40."

The same procedure was performed for the cover, cataloging this variable over five groups measured in intervals of 20 over 20 units, with the first called "cc_00-20" and the last called "cc_80-100".

Finally, the same analysis was performed considering the ranges of slope and cover in relation to the differences in heights in terms of descriptive statistics, RMSE values, box plots, scatterplots, and correlation indexes.

On the other hand, it should be noted that the construction of the GEDI measuring instrument is divided into the three lasers, which are split into four beams that alternate to give eight footprints. The information of which beam has performed the measurement is included in the data of each footprint. Therefore, a detailed analysis of the errors detected has been carried out to explore whether there is any pattern that leads to suggest that some beams are less accurate than others.

2) Zone Statistics: The 12 031 footprints of the study correspond to ten zones with different numbers of footprints, as shown in Table II.

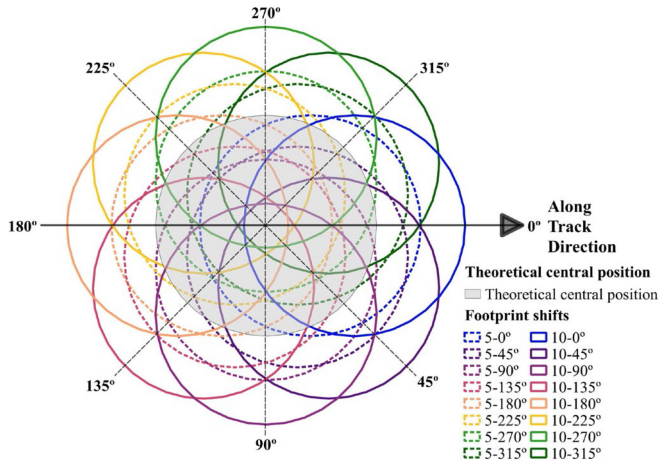

Fig 3. Shifts of GEDI footprints.

As the zones were chosen due to varied vegetation cover, different elevations, and diverse relief characteristics, it should be useful to repeat the same calculations done for the whole set of data, but in this case for each of the ten zones.

The analysis involves considering each zone globally and analyzing it according to the range of slopes and coverage levels described earlier.

D. Uncertainty Analysis

As noted earlier, the location of the GEDI footprint has an uncertainty of ± 10 m. For this reason, errors were estimated between the GEDI metrics and the other two data sources (LiDAR and TDX DEM), shifting the footprints both ± 10 m (maximum error) and ± 5 m (half the maximum error) along and across the satellite orbit and the intermediate angular position between them, depending on the orbit direction (see Fig. 3).

This shifting results in 16 new possible positions where all metrics were extracted following the method described in Section C. Finally, the best footprint location was defined by selecting the one of the 17 possibilities (including the central original position) with lower RMSEs.

IV. RESULTS

A. LiDAR DEMs

Fig. 4 shows the resulting DEM, DSM, and derived slope and canopy cover of the LiDAR data.

B. Statistical Analysis

1) Global Statistics: The global statistics for the four differences in height are shown in Table III. The data show small skewness coefficients, which are fairly symmetrical, and slightly high kurtosis coefficients. The MSE, SD, and RMSE, when comparing the GEDI ELM with the LiDAR data, are slightly lower than when comparing this dataset to the TDX.

Fig. 5 shows the correlation between differences in heights for the global data. A high correlation is observed for all of them except in the case of the RH100 values due to the distribution of the data.

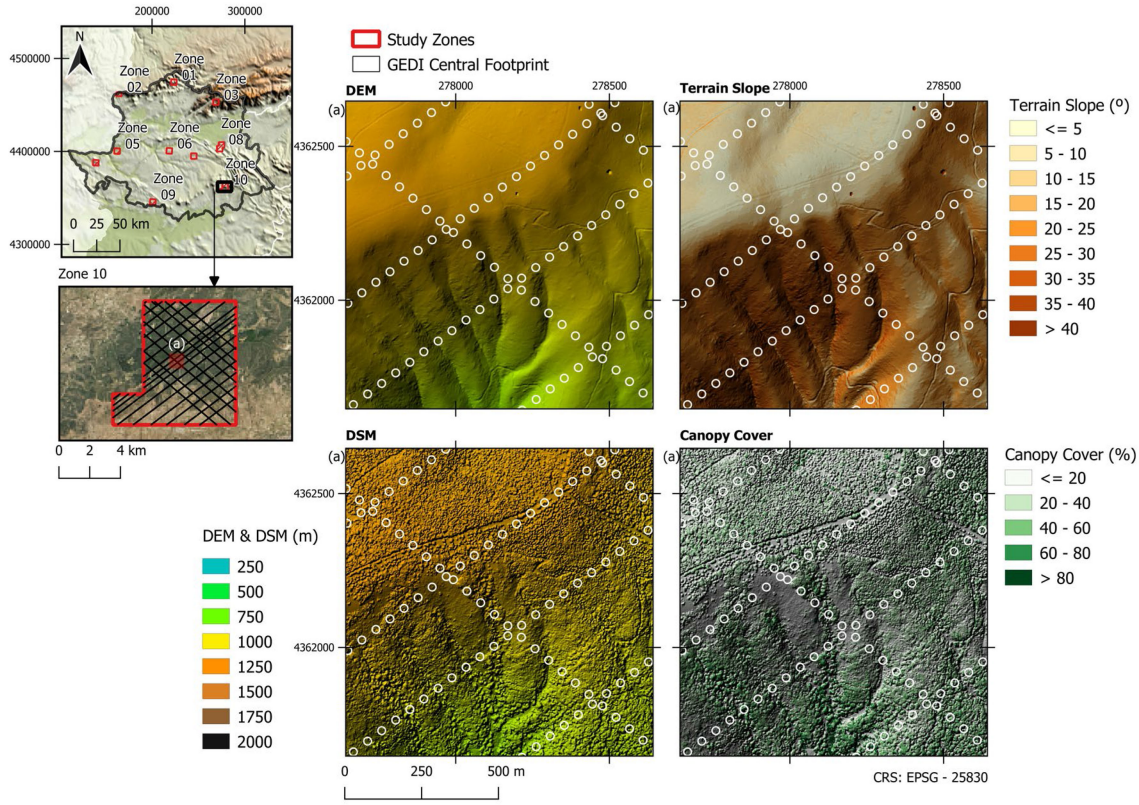

Fig 4. Digital elevation models.

TABLE III
GLOBAL STATISTICS

	ELM G-L	ELM G-T	EHR G-L	RH100 G-L
Mean (m)	0.41	-0.85	0.77	0.35
SD (m)	6.04	6.93	6.44	3.54
MSE (m)	0.05	0.06	0.06	0.03
Median (m)	0.19	-0.63	0.77	0.57
RMSE (m)	6.05	6.99	6.49	3.56
R^2	1.00	1.00	1.00	0.52
IQR	4.61	6.29	5.75	3.50
skewness	0.21	-0.02	-0.59	-0.09
kurtosis	5.35	3.97	3.58	3.18

The calculations of the linear correlation index between each difference in height and the terrain slope and cover do not offer significant values with R^2 values of close to zero.

Fig. 6 shows the RMSE of the four differences in heights for each abovementioned slope range.

In terms of the relation between the terrain slope and RMSE, nearly all comparisons show a positive tendency. In other words, the greater the slope, the greater the RMSE. This trendline has, in the case of the comparison between ELM and GEDI-LiDAR data, a noteworthy value of $R^2 = 0.9926$, and in the case of the comparison between ELM and GEDI-TDX data, a noteworthy value of $R^2 = 0.9892$. For the relation between the terrain slope and the RMSE of the RH100, the trendline is almost horizontal.

Fig. 7 shows boxplots on a scatterplot with the correlations of the ELM G-L and ELM G-T variables and the terrain slope values split by ranges of slopes.

As shown in Figs. 6 and 7, as the slope increases, the differences in elevation are dispersed, especially for slopes of greater than 40, although the dataset of this category is small.

Fig. 8 shows the boxplot for the EHR and RH100 variables. The figure shows more symmetrical distributions due to more proximity between the average mean and median values. According to the comparison with the RH100 metric, it has the lowest IQR value, which denotes less dispersion in differences.

On the other hand, Fig. 9 offers a similar analysis, where the RMSE values obtained from the four differences in heights and cover values split by ranges are plotted.

From the relation between the percentage of vegetation cover and the RMSE and ELM of both comparisons, GEDI-LiDAR and GEDI-TDX show a positive tendency. In other words, the greater the coverage, the greater the RMSE. This relation shows, in the case of the GEDI-LiDAR comparison, a noteworthy value of $R^2 = 0.8870$ for the trendline. Additionally, the RMSE relation for RH100 and cover has also a worthy correlation ($R^2 = 0.8584$ for the trendline).

The boxplots of Fig. 10 show the differences in ELM values between the GEDI and LiDAR data split by cover ranges.

As shown in Figs. 9 and 10, as cover increases, the differences in elevation are dispersed, but not as much as for the slopes. The mean error, when comparing the GEDI ELM to the LiDAR ELM, is lower than when comparing it to the TDX DEM ELM in all cover ranges.

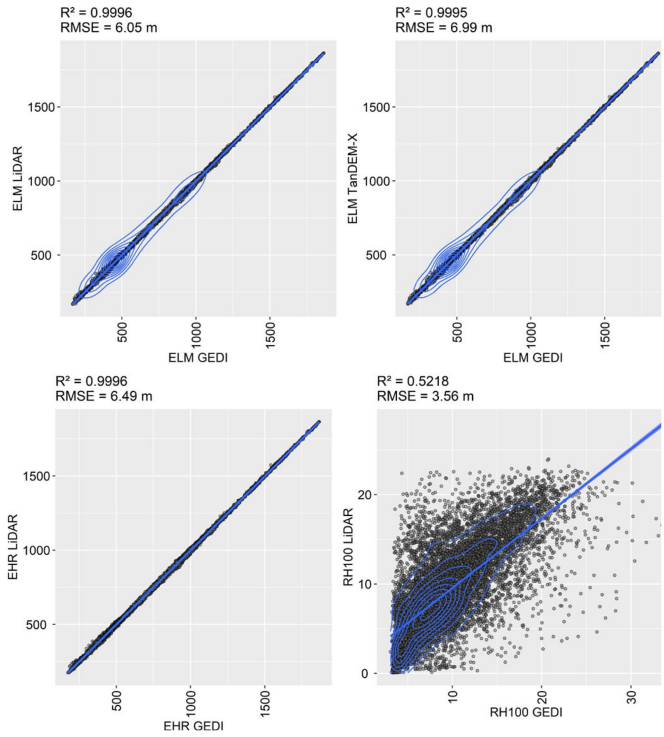

Fig 5. Scatterplots of the differences in heights with RMSE and R^2 values.

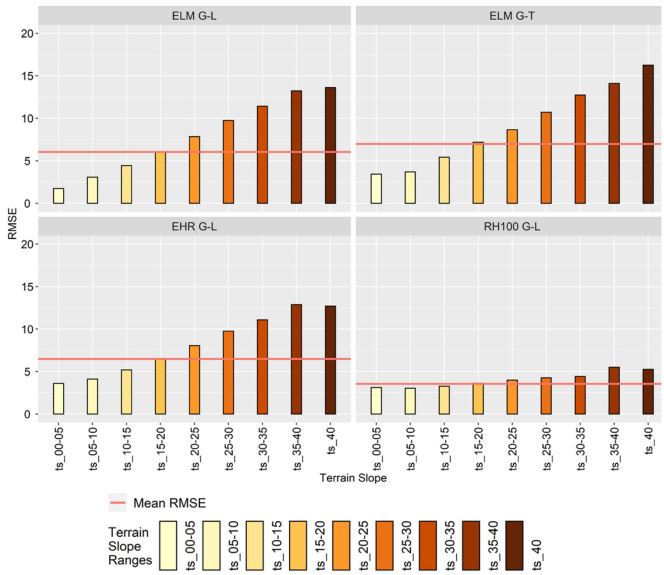

Fig. 6. RMSE of ELM G-L, ELM G-T, EHR G-L, and RH100 G-L values for each slope range.

A similar comparison for the EHR and RH100 values can be observed in Fig. 11.

Fig. 11 shows more concentrated distributions of EHR and RH100 values, especially for the latter. From 20% coverage, the mean difference between the GEDI RH100 and LiDAR data begins to become negative.

Having analyzed the possible influence of the measurement beam of the sensor on the errors committed, it can be seen in Fig. 12 that the beams with the highest errors for ELM are

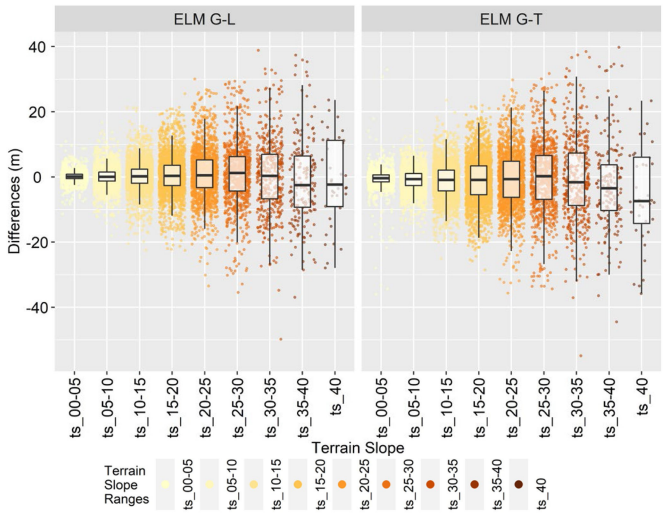

Fig 7. Boxplot on scatterplot of the ELM G-L and ELM G-T variables and the terrain slope values split by ranges.

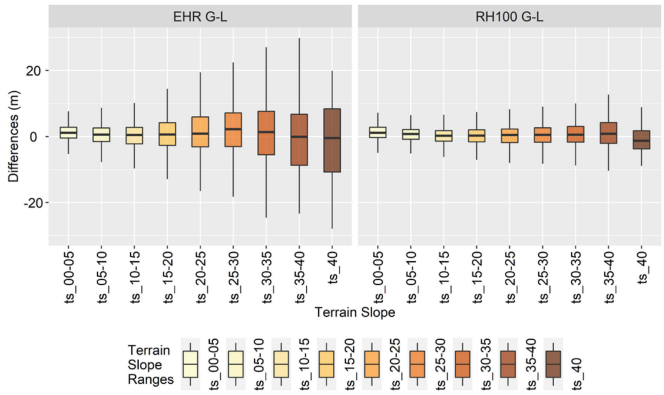

Fig 8. Differences in the EHR between GEDI and LiDAR data for each slope range.

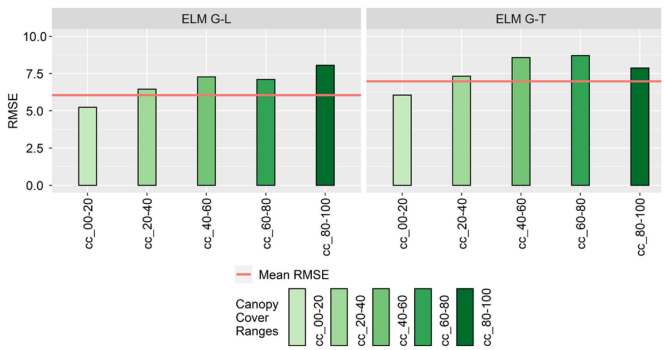

Fig. 9. RMSE of differences between GEDI- LiDAR and GEDI-TDX data for each cover range.

beams B-0000 and B-0011 and that, conversely, those with the lowest RMSE are beams B-1011 and B-1000 in both the GEDI-LiDAR and GEDI-TDX comparisons. For EHR G-L, the tendency is similar, but for RH100 G-L, the tendency is not fulfilled, although in the latter case the differences are very small between the different beams.

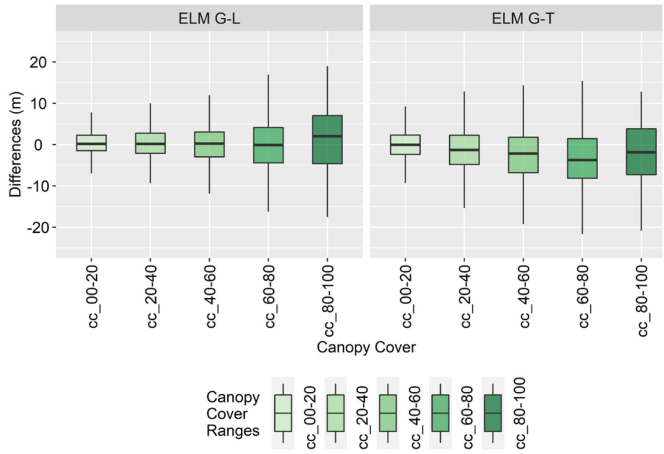

Fig 10. Differences in ELM values between GEDI and LiDAR data and between GEDI and TDX data for each cover range.

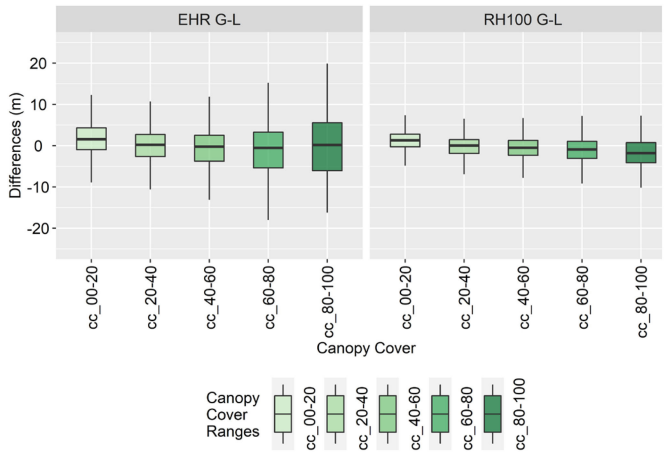

Fig. 11. Differences in EHR and RH100 values between GEDI and LiDAR data for each cover range.

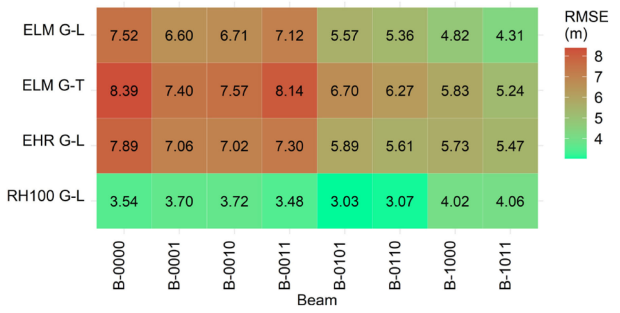

Fig. 12. RMSE in GEDI central footprints for each beam (m).

2) Zone Statistics: A similar analysis was carried out with data from the ten areas into which the study was divided. Fig. 13 displays the RMSE values for each difference in height and zone.

As shown in Fig. 13, the areas with lower RMSE values in general are zones 06 and 07, with RMSE values even lower than 1 m found in the ELM. These values correspond with the two areas with lower mean slopes (see Table I). In contrast, the largest RMSE values correspond with zones 08 and 10, with similar medium both mean slope and mean percentage of cover.

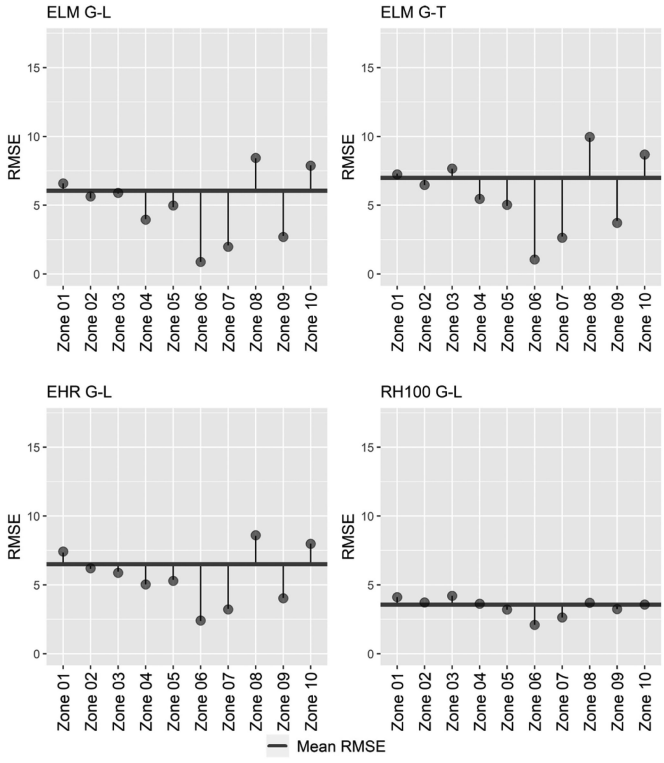

Fig 13. RMSE of differences between GEDI-LiDAR and GEDI-TDX data for each zone.

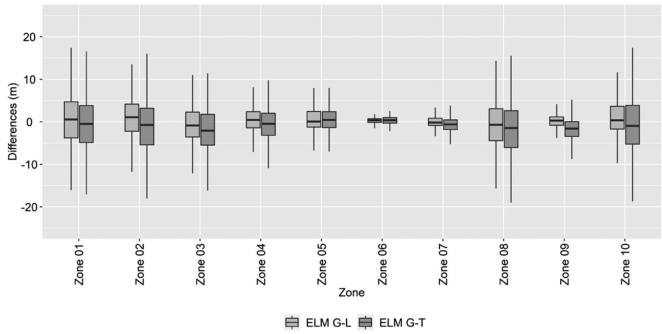

Fig. 14. Differences in ELM values between GEDI-LiDAR and GEDI-TDX data for each zone.

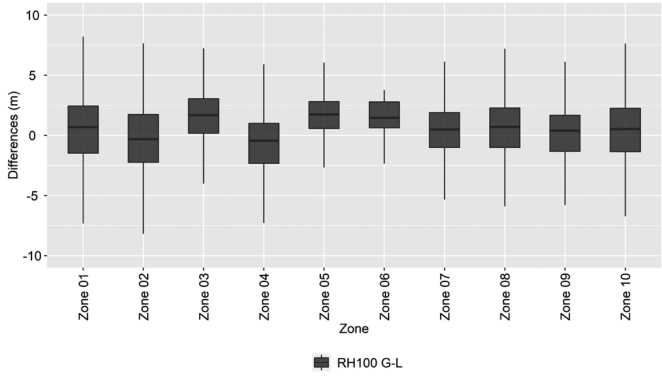

Fig. 15. Differences in RH100 values between GEDI and LiDAR data for each zone.

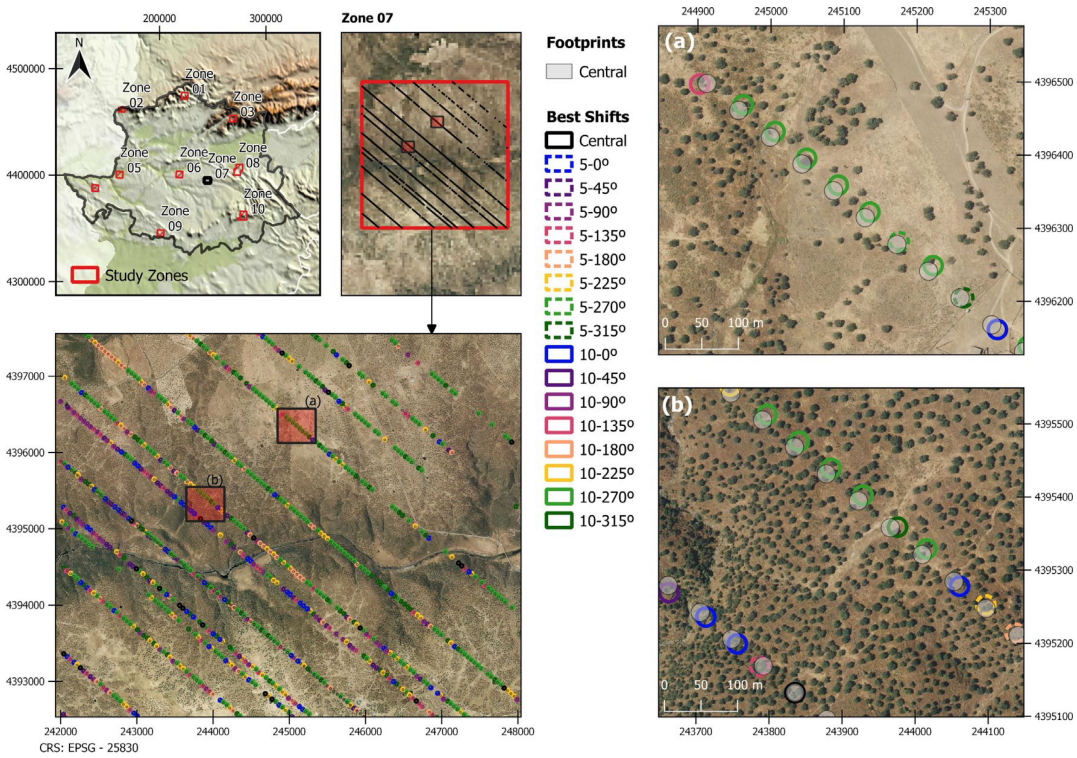

Fig. 16. Best shifts of GEDI footprints relative to LiDAR data. Portion of zone 07 shown as an example.

Additionally, those zones have in common that they both have the higher number of footprints (see Table II).

The boxplots provided in Fig. 14 show the distributions of the ELM differences for the GEDI-LiDAR and GEDI-TDX DEM data.

Figs. 14 and 15 show how in zones 06, 07, and 09, there is much less error dispersion (lower IQR values). These zones correspond to zones of intermediate altitude (450–480 m) and the lowest slopes. Additionally, vegetation coverage is dominated by agroforestry areas.

When comparing the RH100 metric derived from the GEDI with that derived from the LiDAR dataset, we observe more concentrated errors in all zones with IQR values ranging from 2.15 to 4.04 m (see Fig. 15).

It is worth noting that the analysis of zones by slope ranges and cover leads to similar results to the global one. As cover increases, the differences in elevation become dispersed, but not as much as for the slopes. For slopes, the differences in height show more dispersion from a value of 25°, especially for the ELM values. Zones 06 and 07 present nonsignificant results compared to the other zones because their maximum slope values are 11.4° for zone 06 and 37.19° for zone 07.

The RH100 differences offer a more concentrated distribution in all zones and slopes.

Zone 06 has a maximum cover value of 39.86%, and zones 01 and 02 have maximum values of 96.24% and 98.53%, respectively. The remaining zones do not reach the 80% cover value and present a moderate dispersion of the data, which is especially low in the RH100 comparison.

Table IV shows the relation between the RMSE of the RH100 G-L and the RH100 mean value for each zone. It can be observed that the worst values are obtained for zones 05, 06, 07, and 08, where the vegetation height is lower. The best percentage is for zones 01, 02, 03, and 04 with more prominent vegetation in height.

TABLE IV
PERCENTAGE OF RMSE FOR RH100 G-L IN RELATION TO VEGETATION HEIGHT

RMSE	RH100 m	RMSE %
Total	9.19	21.10
Zone 01	10.57	5.08
Zone 02	12.01	6.04
Zone 03	8.30	9.57
Zone 04	9.67	6.98
Zone 05	4.84	15.91
Zone 06	2.99	36.03
Zone 07	6.87	26.27
Zone 08	7.92	44.25
Zone 09	9.69	17.47
Zone 10	11.70	12.79

C. Uncertainty Analysis

1) Global Statistics: The purpose of this section is to find the best location of the footprint once selecting one of the 17 possibilities (central or theoretical location of the footprint and 16 shifts) with less RMSE. As explained in Section III-D, these 16 new proposed footprints are generated by shifting the theoretical position ±10 m and ±5 m along and across the satellite orbit and the intermediate angular position between

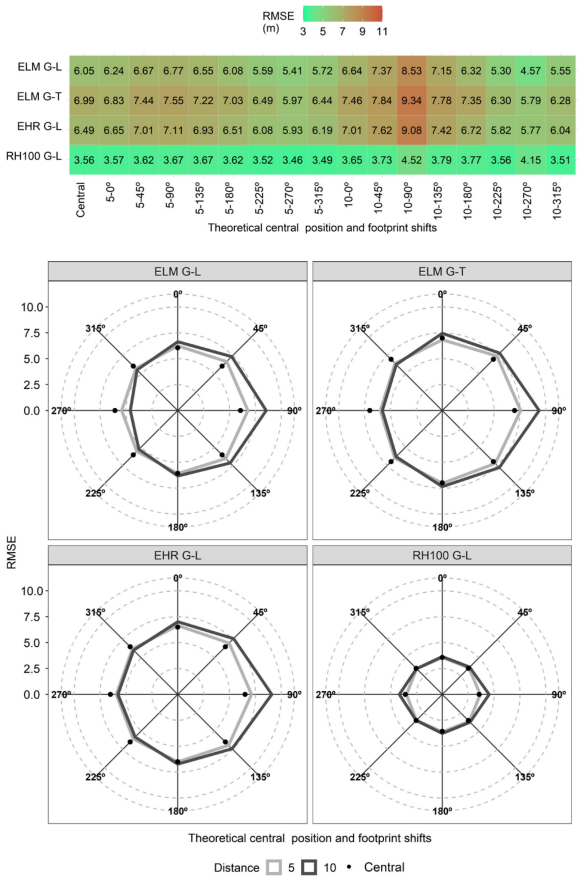

Fig. 17. RMSE of shifts in GEDI footprints (m).

them depending on the orbit direction. According to this, they are called 10-0° Shift, 10-45° Shift, 10-90° Shift, 10-135° Shift 10-180° Shift, 10-225°, 10-270° Shift, and 10-315° Shift for the maximum ±10 m error. In the same way, shifts derived from half the maximum error (±5 m), are called 5-0° Shift, 5-45° Shift, 5-90° Shift, 5-135° Shift, 5-180° Shift, 5-225° Shift, 5-270° Shift, and 5-315° Shift. Fig. 16 shows as an example a portion of zone 07, with the central theoretical position in grey and the best footprint of the 17 possible footprints.

From the RMSE analysis (see Fig. 17), shows that the 10-270° Shift has the lowest values in all comparisons, and the 10-90° Shift has the worst value, except for the RH100 G-L data.

Fig. 18 shows the percentage of GEDI footprints whose heights are best fitted to the ELM LiDAR and ELM TDX elevations, respectively.

From the analysis of the ELM, we find that the percentage of best shifts located at 10-270° is notably larger in both comparisons with LiDAR and TDX data. Fig. 18 shows the 31.88% of the footprints have moved to 10-270° to fit better to the LiDAR ELM data. For TDX data this percentage decreases to 23.60%, but this value is still quite substantial. Furthermore, it should be noted that the central position (theoretical location of the footprint) in both figures has a very low percentage of adjustment in both ELM comparisons. If the 10-270° Shift is the best solution in both cases, the opposite position, the 5-135° Shift, presents the worst results with values of 5.1% and 4.76%, respectively. However, it is worth mentioning that, although this

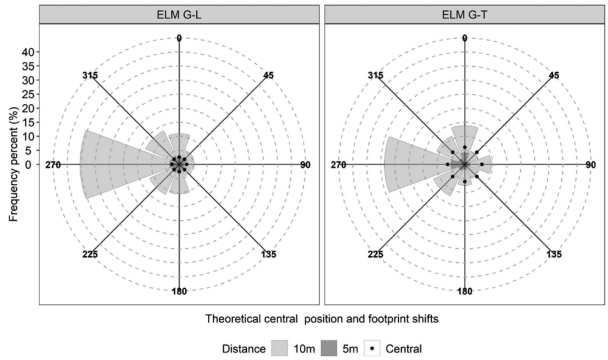

Fig 18. Percentage of shifts of GEDI footprints whose heights are best fitted to the ELM LiDAR elevations and to the ELM TDX elevations.

position of 5-135° Shift and 5-190° Shift are the ones with the fewest quantity of best positions, both in comparison with LiDAR and TDX data, they are not the ones with the highest errors, since, as mentioned above, the one with maximum errors is 10-90° Shift.

As was the case for the theoretical position of the footprint, when the slope increases, the RMSE of the differences in ELM comparisons between GEDI data and LiDAR and TanDEM data increases (see Fig. 19). This increase is more pronounced for 10-90° Shift in both comparisons. Additionally, the results shown in the figures demonstrate that the footprint with less error is the one displaced at 10-270°.

The same study was performed for cover values and is illustrated in Fig. 20. The trend is repeated, and 10-270° Shift offers the best results with lower RMSE values.

2) Zone Statistics: Fig. 21 shows the RMSE values for the four variables considering the theoretical central position and the 16 possible proposed Shift splits by zone.

Zones 06 and 07 are where the RMSE values are most evenly matched between shifts. As noted earlier, these zones correspond to the zones of intermediate altitude (450–480 m) and lowest slope. Additionally, vegetation in these areas is dominated by agroforestry land. On the other hand, zone 01 has the highest RMSEs values. Finally, it should be noted that the 10-270° Shift presents the lowest RMSE in all zones and, similarly, 10-90° Shift has the highest RMSE values in all zones.

V. Discussion

In our analysis, the real elevations and heights captured by the GEDI sensor have been compared to other Airborne and Spaceborne data sources. LiDAR-derived DEM data and DSM and TanDEM-DEM data were utilized to draw comparisons due to their greater accuracy. We also compared both sources of information to quantify the differences in elevation between them. Similar contrasts can be found in the recent literature. Wessel *et al.* [35] compared the LiDAR DEM and TDX DEM and obtained a global RMSE of 6.78 m. The authors also calculated the error within several slope ranges and found that the steeper the slope, the higher the RMSE. We obtained an overall RMSE for differences between the LiDAR-derived DEM and TDX DEM of 3.35 m, a value that is much lower and, therefore, shows a better fit between the data sources with which we compared

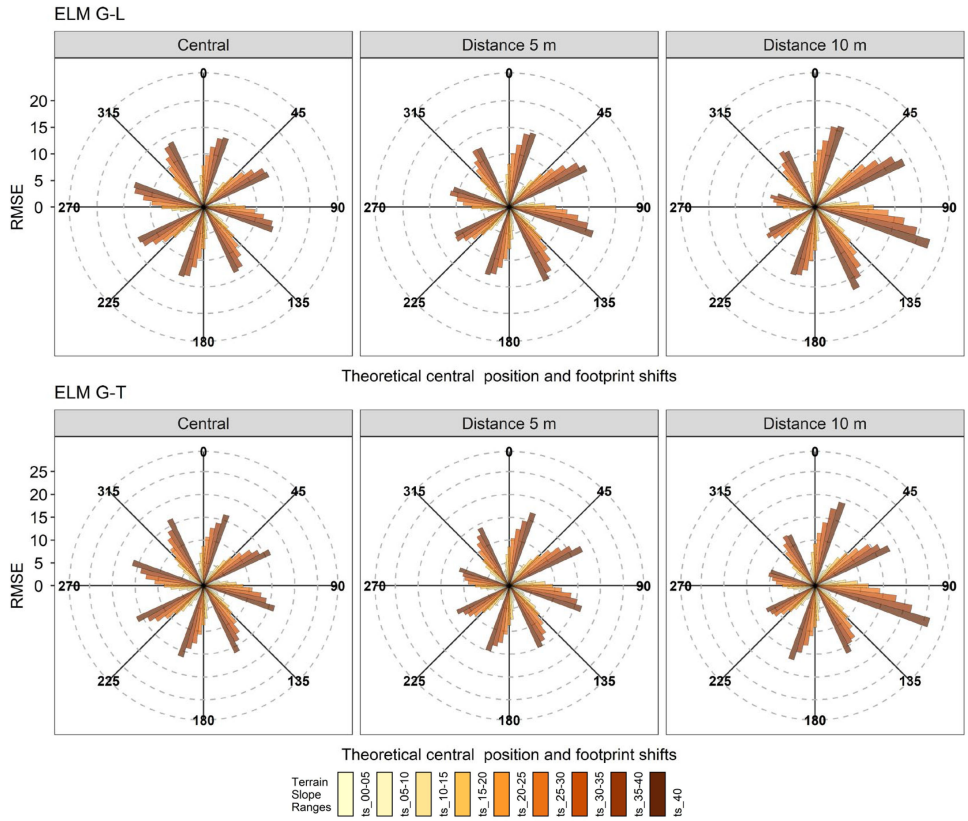

Fig. 19. RMSE variation of theoretical footprints and shifts of ELM comparisons for GEDI and LiDAR data.

GEDI elevations and heights. As Wessel *et al.* [35], we also found the error to increase with the slope of terrain (see Fig. 22). Additionally, we analyzed trends that occur with an increase in coverage and found that the greater the coverage, the greater the RMSE (see Fig 22). In both cases, all RMSEs comply with the TDX Ground Segment DEM Products Specification Document [56], which indicates an absolute vertical accuracy value of less than 10 m.

It is worth noting that the TDX DEM reproduces a surface model that includes above ground elevation tree canopies and built elements, which supports the positive trend of the RMSE related to coverage. However, as stated in Wessel *et al.* [35], the mean errors for aboveground land cover classes are lower than expected for an interferometric SAR system such as TDX. In this sense, the TDX Ground Segment DEM Products Specification Document [56] confirms that in forested areas, the *X*-band SAR scattering center is located closer to the upper part of the vegetation volume rather than on the crown itself. Consequently, it can be considered, in almost all extensions, a measure of ground elevation. This conclusion is supported by recent works such as that by Chimitdorzhiev *et al.* [38], who found an error in canopy height, concluding that radar interferometric measurements underestimate the actual forest height by an average value of 5.5 m for high coverage and by 2–4 m for medium coverage. On the other hand, Gonzalez and Rizzoli [57] summarized the global relative height accuracy of the global TDX DEM for all continents and cover types. In our case, for Europe, the authors set accuracy levels of 1.64 m for forests, of 0.94 m for short vegetation, and of 0.96 for shrubland, which account for most of our cover categories.

In terms of the main results of this work, we obtained an RMSE of 6.05 m when comparing the ELM of GEDI and LiDAR data and an RMSE of 6.99 when comparing GEDI and TDX data, but with an almost perfect correlation R^2 between them (0.9996 and 0.9995). Such values of a nearly perfect correlation were also obtained by Silva *et al.* [45], but they obtained better RMSE results. These differences can be attributed to the fact that they used simulated data while we used real data. However, although from the global data our RMSE does not reach the values that Silva *et al.* [45] obtained, for zones 06, 07, and 09, we do obtain RMSE values that fall within the range of their results (0.89–2.77 m) or that are even better.

Other notable results are those achieved for the RH100 metric. In the global results, we obtained an RMSE of 3.56 m. Qi and Dubayah [50] obtained RMSE values ranging from 3.53 to 12.59 m when comparing RH100 values derived from different comparisons of LiDAR metric measurements with a combination of TDX and (synthetic) GEDI data. These results are in accordance with those obtained in this work, for both the original position of the footprint and most of its shifts, which are at the lower limit of their RMSE range.

In the same way, Hancock *et al.* [46] assessed the accuracy of the GEDI simulator, which underpins the prelaunch calibration of GEDI data products. The authors calculated differences in RH2, RH5, RH25, RH50, RH75, and RH98 metrics compared to ALS datasets and obtained RMSEs of approximately 4.7–5.7

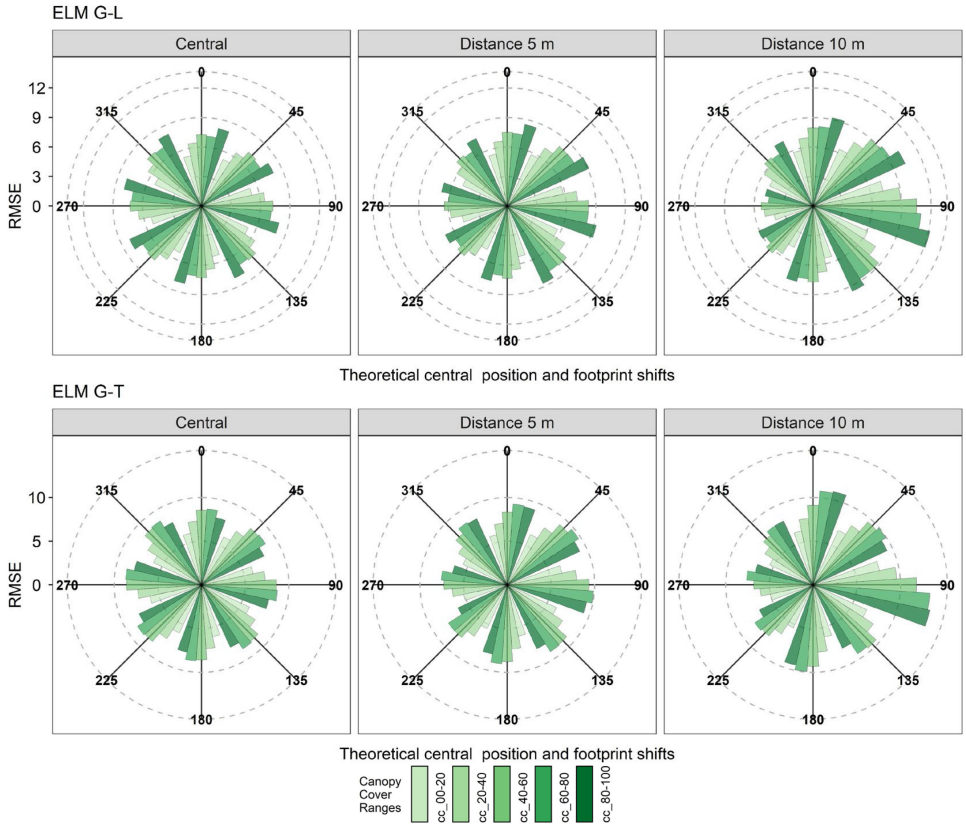

Fig. 20. RMSE variations of theoretical footprints and shifts of ELM comparisons for GEDI and TDX data.

m. We obtained better results in all the studied zones, with a minimum value in Zone 06 of 2.09 that is even less than half their minimum RMSE. Healey *et al.* [40] also performed RH98 predictions at 7615 focal sites using models calibrated at three scales, obtaining RMSEs ranging from 7.08 to 9.2 m and IQR values of 6.89–11.19 m. Our general results show a significantly better general IQR of 3.50 m for RH100 differences and values ranging from 2.15 to 4.04 m. If we focus on the percentages of the RMSE with respect to the RH100 value, our values are also better than those of Healey *et al.* [40] since our maximum RMSE% (44%) is their minimum and we have zones with errors up to five times better than this error (zone 01). The highest RMSE% were found in areas with the lower vegetation. Additionally, in analyzing RH98 differences per vegetation type, Healey *et al.* [40] achieved a minimum RMSE of 4.50 m for grasslands with the minimum work scale and a maximum RMSE of 10.58 m for evergreen broadleaf forests with the maximum work scale. We achieved a minimum RMSE of 2.09 m for the RH100 for zone 06 (agroforestry areas) and a maximum RMSE of 4.20 m for zone 03 (sclerophyllous vegetation). Globally, the RMSE obtained for the RH100 is 3.56 m, which is in accordance with the minimum general result given by Healey *et al.* [40].

With regard to the EHR, our results achieve an RMSE of 6.49 m globally. In general, these altitudes generated the worst results of all of the work in spite of the fact that in zone 06 they reached better values with an RMSE of 2.37 m. None of the consulted studies using GEDI data provide results in on the elevations of the highest points of vegetation, so we cannot draw comparisons.

On the other hand, we used only elevations of footprints with a quality flag of 1 to ensure the quality of the elevation data. Fayad *et al.* [20] used flag 0 or 1 to analyze the elevation of inland waterbodies and applied an elevation filter with SRTM elevations. Although they achieved more accurate results (studying areas without vegetation, without which there is less scope for confusing elevation), they noticed an improvement when applying the SRTM filter to the elevations, even for footprints with a quality flag of 1.

As stated in Luthcke *et al.* [49], the GEDI instrument consists of three lasers producing a total of eight beam ground transects. These three lasers are as follows: the "coverage" laser and two full power lasers. The "coverage" laser is split into two transects that are then each dithered producing four ground transects. The other two lasers are dithered only, producing two ground transects each. In our study area, beams B-0000, B-0001, B-0010, and B-0011, correspond to the "coverage" laser and beams B-0101, B-0110, B-1000, and B-1011, correspond to the other full power lasers. Thus, it can be clearly seen how the coverage laser has more error than the other two lasers for the EHR G-L, ELM G-L, and ELM G-T. Nevertheless, it can be seen that for RH100 G-L, one of the two full power laser beams is the one with the lower RMSE.

Finally, in terms of our evaluation of the uncertainty of the footprint location, we obtained better results for almost 35% of our 12 031 footprints when shifting them 10 m and 270° in the orbit direction. Most of the literature using GEDI data works with simulated data. Using simulated GEDI data at precise

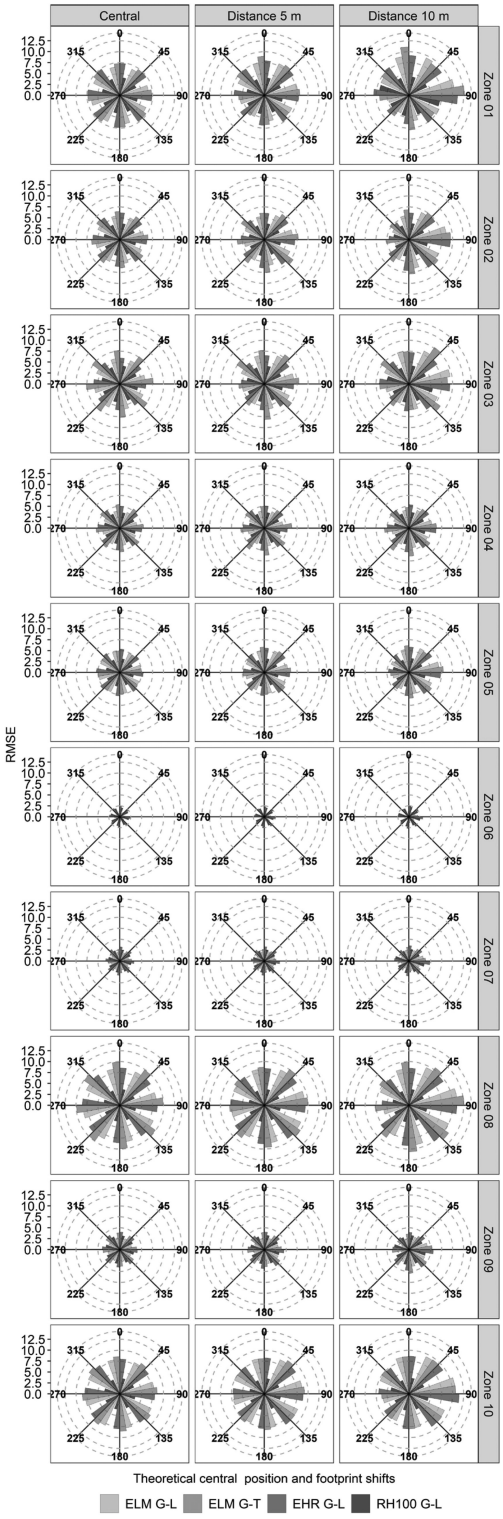

Fig. 21. RMSE for all comparisons drawn for theoretical positions and shifts of GEDI footprints by zone.

locations to build footprint-level models obviates potential errors related to the positional uncertainty of GEDI footprints of ± 10 m [58]. As stated by Luthcke *et al.* [49], the intention is for GEDI mission geolocation to occur within the same frame and to use consistent geophysical corrections similar to those

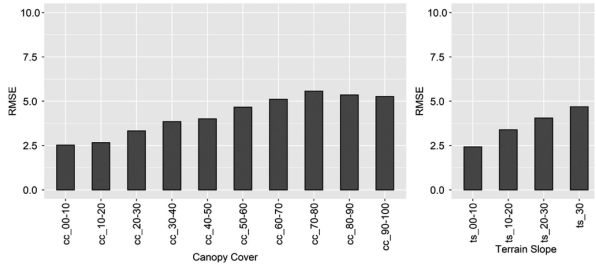

Fig. 22. RMSE of differences between TDX and LiDAR data for different vegetation cover factors and slope ranges.

of ICESat-2 to facilitate the direct comparison and use of these laser altimeter mission data. The fusion approach applying GEDI and TDX data shows great potential for generating global-scale forest and biomass maps [43].

Despite being rather dense, with the comparison of 12 031 footprints and their respective parallels that have resulted in the study of 204 527 locations, the assessment carried out in this study, has been automated by means of *R* scripts and GIS programming, achieving an exhaustive analysis of the errors between the three sources of data studied. For further validation studies of GEDI with airborne LiDAR data, it would be recommended to establish a mathematical transformation model between both data sources for a correct extrapolation of the valuable information from GEDI data. It would also be advisable to explore the theory of authors such as Potapov *et al.* [59] or Lang *et al.* [60] who indicate that such extrapolation could be carried out using multispectral images such as those of Landsat, Sentinel, or many others.

VI. Conclusion

In this study, we compared real GEDI elevation data with other airborne and spaceborne DEM data for Southwest Spain. We analyzed agreement in ground elevation (ELM) across 12 031 real GEDI footprints and elevations obtained from LiDAR and TDX DEM data. In general, we achieved better agreement with the LiDAR data. Additionally, a comparison of the RH100 metric and the elevation of the highest point of vegetation (EHR) obtained from GEDI and LiDAR data was performed. In this case, the obtained results are in substantial agreement with other studies using simulated GEDI data.

Furthermore, the results show a clear relation between the errors obtained and the slope; the greater the slope, the greater the RMSE. This relationship has also been found by analyzing different degrees of coverage; as cover increases, differences in elevation become dispersed, but not as much as with slopes.

Finally, due to our initial predictions of uncertainty in GEDI footprints, a final evaluation of RMSE involved shifting 16 footprints in the ± 10 m uncertainty area. The obtained outcomes evidence a strong tendency to obtain better results (in terms of RMSE and frequency) on ground elevation when placing the footprint at 270°, displacing it to 10 m of its positional uncertainty, from comparative studies of LiDAR and TDX data.

The global results of this work show differences in elevation in relation to other data sources. These differences may or may not be important depending on the scale of work and the accuracy of

forest mapping required. However, as it appears that future plans for the GEDI mission are to be placed within the same frame and to use consistent geophysical corrections similar to those of ICESat-2, improved positional uncertainty and height accuracy are to be expected. Following this, it would be highly desirable to conduct a new accuracy assessment of GEDI elevations to see if and by how much the differences found in this study vary. Additionally, many of our investigations point to a combination of GEDI data with TDX data to overcome the limitations of GEDI point sampling. This combination will also greatly reduce the differences between the two data sources. Future research is, therefore, needed to establish transformation models between these data sources.

ACKNOWLEDGMENT

The authors would like to thank the Junta de Extremadura (CICTEX) for providing the LiDAR data (LiDAR-PNOA 2018 CC-BY 4.0 scne.es). They also would like to thank the German Aerospace Centre (DLR) for providing TerraSAR-X/TanDEM-X © DLR <2020> satellite data.

REFERENCES

[1] S. C. Popescu, K. Zhao, A. Neuenschwander, and C. Lin, "Satellite lidar vs. small footprint airborne lidar: Comparing the accuracy of aboveground biomass estimates and forest structure metrics at footprint level," *Remote Sens. Environ.,* vol. 115, pp. 2786–2797, 2011.

[2] X. Yu *et al.*, "Comparing features of single and multi-photon lidar in boreal forests," *ISPRS J. Photogrammetry Remote Sens.,* vol. 168, pp. 268–276, 2020.

[3] M. Dalponte *et al.*, "Aboveground biomass estimation in tropical forests at single tree level with ALS data," in *Proc. IEEE Int. Geosci. Remote Sens. Symp.*, Beijing, China, 2016, pp. 5334–5337.

[4] F. J. Romero Ramirez, R. M. Navarro-Cerrillo, M. Á. Varo-Martínez, J. L. Quero, S. Doerr, and R. Hernández-Clemente, "Determination of forest fuels characteristics in mortality-affected Pinus forests using integrated hyperspectral and ALS data," *Int. J. Appl. Earth Observ. Geoinf.,* vol. 68, pp. 157–167, 2018.

[5] M. Dalponte, H. O. Ørka, L. T. Ene, T. Gobakken, and E. Næsset, "Tree crown delineation and tree species classification in boreal forests using hyperspectral and ALS data," *Remote Sens. Environ.,* vol. 140, pp. 306–317, 2014.

[6] A. Harikumar, C. Paris, F. Bovolo, and L. Bruzzone, "A crown quantization-based approach to tree-species classification using high-density airborne laser scanning data," *IEEE Trans. Geosci. Remote Sens.,* vol. 59, no. 5, pp. 4444–4453, May 2021.

[7] I. Arenas-Corraliza, A. Nieto, and G. Moreno, "Automatic mapping of tree crowns in scattered-tree woodlands using low-density LiDAR data and infrared imagery," *Agroforestry Syst.,* vol. 94, pp. 1989–2002, 2020.

[8] L. Fragoso-Campón, E. Quirós, J. Mora, J. A. Gutiérrez Gallego, and P. Durán-Barroso, "Overstory-understory land cover mapping at the watershed scale: Accuracy enhancement by multitemporal remote sensing analysis and LiDAR," *Environ. Sci. Pollut. Res.,* vol. 27, pp. 75–88, 2020.

[9] A. Neuenschwander, E. Guenther, J. C. White, L. Duncanson, and P. Montesano, "Validation of ICESat-2 terrain and canopy heights in boreal forests," *Remote Sens. Environ.,* vol. 251, 2020, Art. no. 112110.

[10] L. L. Narine, S. Popescu, A. Neuenschwander, T. Zhou, S. Srinivasan, and K. Harbeck, "Estimating aboveground biomass and forest canopy cover with simulated ICESat-2 data," *Remote Sens. Environ.,* vol. 224, pp. 1–11, 2019.

[11] W. Li, Z. Niu, R. Shang, Y. Qin, L. Wang, and H. Chen, "High-resolution mapping of forest canopy height using machine learning by coupling ICESat-2 LiDAR with Sentinel-1, Sentinel-2 and Landsat-8 data," *Int. J. Appl. Earth Observ. Geoinf.,* vol. 92, 2020, Art. no. 102163.

[12] F. D. Schneider *et al.*, "Towards mapping the diversity of canopy structure from space with GEDI," *Environ. Res. Lett.,* vol. 15, 2020, Art. no. 115006.

[13] R. Dubayah *et al.*, "The global ecosystem dynamics investigation: High-resolution laser ranging of the earth's forests and topography," *Sci. Remote Sens.,* vol. 1, 2020, Art. no. 100002.

[14] L. Duncanson *et al.*, "Biomass estimation from simulated GEDI, ICESat-2 and NISAR across environmental gradients in Sonoma county, California," *Remote Sens. Environ.,* vol. 242, 2020, Art. no. 111779.

[15] N. Sanchez-Lopez, L. Boschetti, A. T. Hudak, S. Hancock, and L. I. Duncanson, "Estimating time since the last stand-replacing disturbance (TSD) from spaceborne simulated GEDI data: A feasibility study," *Remote Sens.,* vol. 12, 2020, Art. no. 3506.

[16] W. Qi, S. Saarela, J. Armston, G. Ståhl, and R. Dubayah, "Forest biomass estimation over three distinct forest types using TanDEM-X InSAR data and simulated GEDI lidar data," *Remote Sens. Environ.,* vol. 232, 2019, Art. no. 111283.

[17] W. Qi *et al.*, "Improved forest height estimation by fusion of simulated GEDI lidar data and TanDEM-X InSAR data," *Remote Sens. Environ.,* vol. 221, pp. 621–634, 2019.

[18] S. M. Marselis *et al.*, "Exploring the relation between remotely sensed vertical canopy structure and tree species diversity in Gabon," *Environ. Res. Lett.,* vol. 14, 2019, Art. no. 094013.

[19] P. B. Boucher *et al.*, "Detecting change in forest structure with simulated GEDI lidar waveforms: A case study of the Hemlock woolly adelgid (HWA; adelges tsugae) infestation," *Remote Sens.,* vol. 12, 2020, Art. no. 1304.

[20] I. Fayad, N. Baghdadi, J. S. Bailly, F. Frappart, and M. Zribi, "Analysis of GEDI elevation data accuracy for inland waterbodies altimetry," *Remote Sens.,* vol. 12, 2020, Art. no. 2714.

[21] G. V. Laurin, F. Del Frate, L. Pasolli, and C. Notarnicola, "Forest/vegetation types discrimination in an alpine area using RADARSAT2 and ALOS PALSAR polarimetric data and neural networks," in *Proc. IEEE Int. Geosci. Remote Sens. Symp.*, Munich, Germany, 2012, pp. 5340–5343.

[22] C. Wecklich, M. Martone, P. Rizzoli, J.-L. Bueso-Bello, C. Gonzalez, and G. Krieger, "Production of a global forest/non-forest map utilizing TanDEM-X interferometric SAR data," in *Proc. IEEE Int. Geosci. Remote Sens. Symp.*, 2017, pp. 751–754.

[23] C. N. Koyama, M. Watanabe, M. Hayashi, T. Ogawa, and M. Shimada, "Mapping the spatial-temporal variability of tropical forests by ALOS-2 L-band SAR big data analysis," *Remote Sens. Environ.,* vol. 233, 2019, Art. no. 111372.

[24] M. Martone *et al.*, "The global forest/non-forest map from TanDEM-X interferometric SAR data," *Remote Sens. Environ.,* vol. 205, pp. 352–373, 2018.

[25] A. P. Nicolau, A. Flores-Anderson, R. Griffin, K. Herndon, and F. J. Meyer, "Assessing SAR C-band data to effectively distinguish modified land uses in a heavily disturbed Amazon forest," *Int. J. Appl. Earth Observ. Geoinf.,* vol. 94, 2020, Art. no. 102214.

[26] A. Toraño Caicoya, F. Kugler, M. Pardini, I. Hajnsek, and K. Papathanassiou, "Vertical forest structure characterization for the estimation of above ground biomass: First experimental results using SAR vertical reflectivity profiles," in *Proc. IEEE Int. Geosci. Remote Sens. Symp.*, Québec city, QC, Canada, 2014, pp. 1045–1048.

[27] A. Kumar *et al.*, "Tree diversity assessment and above ground forests biomass estimation using SAR remote sensing: A case study of higher altitude vegetation of north-east Himalayas, India," *Phys. Chem. Earth, Parts A/B/C,* vol. 111, pp. 53–64, 2019.

[28] Z. Liao, B. He, and X. Quan, "Potential of texture from SAR tomographic images for forest aboveground biomass estimation," *Int. J. Appl. Earth Observ. Geoinf.,* vol. 88, 2020, Art. no. 102049.

[29] Y. Liu, W. Gong, Y. Xing, X. Hu, and J. Gong, "Estimation of the forest stand mean height and aboveground biomass in northeast china using SAR Sentinel-1B, multispectral Sentinel-2A, and DEM imagery," *ISPRS J. Photogrammetry Remote Sens.,* vol. 151, pp. 277–289, 2019.

[30] A. L. Mitchell, A. Rosenqvist, and B. Mora, "Current remote sensing approaches to monitoring forest degradation in support of countries measurement, reporting and verification (MRV) systems for REDD+," *Carbon Balance Manage.,* vol. 12, 2017, Art. no. 9.

[31] J. Ruiz-Ramos, A. Marino, C. Boardman, and J. Suarez, "Continuous forest monitoring using cumulative sums of Sentinel-1 timeseries," *Remote Sens.,* vol. 12, 2020, Art. no. 3061.

[32] X. Wang, Y. Zhang, P. M. Atkinson, and H. Yao, "Predicting soil organic carbon content in Spain by combining Landsat TM and ALOS PALSAR images," *Int. J. Appl. Earth Observ. Geoinf.,* vol. 92, 2020, Art. no. 102182.

[33] B. O. Tagnon, V. T. Assoma, J. M. O. Mangoua, A. G. Douagui, F. K. Kouamé, and I. Savané, "Contribution of SAR/RADARSAT-1 and ASAR/ENVISAT images to geological structural mapping and assessment of lineaments density in Divo-Oume area (Côte d'Ivoire)," *Egyptian J. Remote Sens. Space Sci.,* vol. 23, pp. 231–241, 2018.
[34] A. Mazza, F. Sica, P. Rizzoli, and G. Scarpa, "TanDEM-X forest mapping using convolutional neural networks," *Remote Sens.,* vol. 11, 2019, Art. no. 2980.
[35] B. Wessel, M. Huber, C. Wohlfart, U. Marschalk, D. Kosmann, and A. Roth, "Accuracy assessment of the global TanDEM-X digital elevation model with GPS data," *ISPRS J. Photogrammetry Remote Sens.,* vol. 139, pp. 171–182, 2018.
[36] L. Hawker, J. Neal, and P. Bates, "Accuracy assessment of the TanDEM-X 90 digital elevation model for selected floodplain sites," *Remote Sens. Environ.,* vol. 232, 2019, Art. no. 111319.
[37] V. Vanthof and R. Kelly, "Water storage estimation in ungauged small reservoirs with the TanDEM-X DEM and multi-source satellite observations," *Remote Sens. Environ.,* vol. 235, 2019, Art. no. 111437.
[38] T. Chimitdorzhiev, A. Dmitriev, I. Kirbizhekova, A. Sherkhoeva, A. Baltukhaev, and P. Dagurov, "Possible inaccuracy of canopy height model estimation for dense and sparse boreal forest with Tandem-X DSM and ALOS palsar DEM fusion, case study from the Baikal lake region, Russia," in *Proc. IEEE Int. Geosci. Remote Sens. Symp.*, Yokohama, Japan, 2019, pp. 6693–6695.
[39] R. Dubayah *et al.*, "GLOBAL ecosystem dynamics investigation (GEDI) level 02 user guide," Jan. 2020. Online. [Available]: https://lpdaac.usgs.gov/documents/650/GEDI02_UserGuide_V1.pdf
[40] S. P. Healey, Z. Yang, N. Gorelick, and S. Ilyushchenko, "Highly local model calibration with a new GEDI LiDAR asset on Google earth engine reduces landsat forest height signal saturation," *Remote Sens.,* vol. 12, 2020, Art. no. 2840.
[41] S.-K. Lee, T. Fatoyinbo, W. Qi, S. Hancock, J. Armston, and R. Dubayah, "GEDI and TanDEM-X fusion for 3D forest structure parameter retrieval," in *Proc. IEEE Int. Geosci. Remote Sens. Symp.*, Valencia, Spain, 2018, pp. 380–382.
[42] C. Choi, M. Pardini, and K. Papathanassiou, "A structure-based framework for the combination of GEDI and Tandem-X measurements over forest scenarios," in *Proc. IEEE Int. Geosci. Remote Sens. Symp.*, Yokohama, Japan, 2019, pp. 4488–4490.
[43] S.-K. Lee *et al.*, "Spaceborne data fusion for large-scale forest parameter estimation: GEDI lidar & Tandem-X INSAR missions," in *Proc. IEEE Int. Geosci. Remote Sens. Symp.*, Yokohama, Japan, 2019, pp. 4491–4494.
[44] W. Qi and R. O. Dubayah, "Forest structure modeling of a coniferous forest using TanDEM-X InSAR and simulated GEDI lidar data," in *Proc. IEEE Int. Geosci. Remote Sens. Symp.*, Fort Worth, TX, USA, 2017, pp. 914–917.
[45] C. A. Silva *et al.*, "Comparison of small-and large-footprint lidar characterization of tropical forest aboveground structure and biomass: A case study from central Gabon," *IEEE J. Sel. Topics Appl. Earth Observ. Remote Sens.,* vol. 11, no. 10, pp. 3512–3526, Oct. 2018.
[46] S. Hancock *et al.*, "The GEDI simulator: A large-footprint waveform lidar simulator for calibration and validation of spaceborne missions," *Earth Space Sci.,* vol. 6, pp. 294–310, 2019.
[47] A. Kato, H. Wakabayashi, M. Bradford, A. Hudak, L. M. Moskal, and M. Watanabe, "Accurate ground positioning obtained from 3d data matching between airborne and terrestrial data for ground validation of satellite laser," in *Proc. IEEE Int. Geosci. Remote Sens. Symp.*, Yokohama, Japan, 2019, pp. 6632–6635.
[48] S. Rivas-Martinez and S. Rivas-Saenz, Worldwide Bioclimatic Classification System. Jul. 2019. [Online]. Available: http://www.globalbioclimatics.org/form/tb_map/index.htm
[49] S. B. Luthcke, T. Rebold, T. Thomas, and T. Pennington, "Algorithm theoretical basis document (ATBD) for GEDI waveform geolocation for L1 and L2 products," 2019. Online. [Available]: https://lpdaac.usgs.gov/documents/579/GEDI__WFGEO_ATBD_v1.0.pdf
[50] W. Qi and R. O. Dubayah, "Combining Tandem-X InSAR and simulated GEDI lidar observations for forest structure mapping," *Remote Sens. Environ.,* vol. 187, pp. 253–266, 2016.
[51] National Centre for Geographic Information, "Technical Specifications of the National Aerial Orthophotography Plan," (in Spanish), 2018. Online. [Available]: https://pnoa.ign.es/especificaciones-lidar
[52] C. A. Silva *et al.*, "rGEDI: NASA's global ecosystem dynamics investigation (GEDI) data visualization and processing," R package version 0.1.7 ed, 2020. [Online]. Available: https://github.com/carlos-alberto-silva/rGEDI
[53] R. J. McGaughey, *FUSION/LDV: Software for LIDAR Data Analysis and Visualization*, U.S. Department of Agriculture: Forest Service, Pacific Northwest Research Station, Seattle, WA, USA, 2009.
[54] R. J. McGaugheey, "Manual FUSION/LDV Software for LiDAR Data Analysis and Visualization," 2020. Online. [Available]: http://forsys.cfr.washington.edu/fusion/fusionlatest.html
[55] R-Core-Team, "R: A language and environment for statistical computing," R Foundation for Statistical Computing, Vienna, Austria, 2018. Online. [Available]: https://www.R-project.org/
[56] B. Wessel, T. Fritz, and G. Krieger, "TanDEM-X Ground Segment DEM Products Specification Document," 2016. Online. [Available]: https://elib.dlr.de/108014/1/TD-GS-PS-0021_DEM-Product-Specification_v3.1.pdf
[57] C. Gonzalez and P. Rizzoli, "Landcover-dependent assessment of the relative height accuracy in TanDEM-X DEM products," *IEEE Geosci. Remote Sens. Lett.,* vol. 15, no. 12, pp. 1892–1896, Dec. 2018.
[58] P. L. Patterson *et al.*, "Statistical properties of hybrid estimators proposed for GEDI—NASA's global ecosystem dynamics investigation," *Environ. Res. Lett.,* vol. 14, 2019, Art. no. 065007.
[59] P. Potapov *et al.*, "Mapping global forest canopy height through integration of GEDI and Landsat data," *Remote Sens. Environ.,* vol. 253, 2021, Art. no. 112165.
[60] N. Lang, K. Schindler, and J. D. Wegner, "Country-wide high-resolution vegetation height mapping with Sentinel-2," *Remote Sens. Environ.,* vol. 233, 2019, Art. no. 111347.

Elia Quirós was born in 1972 in Cáceres, Spain. She received the Technical Engineering degree in topography, the engineering degree in geodesy and cartography, and the Ph.D. degree in geodesy and cartography from the University of Extremadura, Badajoz, Spain, in 1999, 2001, and 2009, respectively.

She is currently an Associate Professor of Digital Photogrammetry with the Polytechnic School, and of Remote Sensing with the Faculty of Philosophy and Arts, both with the University of Extremadura. She is the author of 3 books and 22 articles. Her published works are related to remote sensing and spatial photogrammetry.

Dr. Quirós is a member of the Spanish Society of Remote Sensing and she is the Head of the SNAP (Sentinel Application Platform) Working Group.

María-Eugenia Polo was born in Mérida, Spain, in 1968. She received the Technical Engineering degree in surveying from the University of Extremadura, Badajoz, Spain, in 1990, the Engineering degree in geodesy and cartography from the University of Jaén, Jaén, Spain, in 2000, and the Ph.D. degree in geodesy and cartography from the University of Extremadura, in 2008.

She is currently an Associate Professor of Geomatics and Surveying with the University Centre of Mérida, University of Extremadura. She is the author of 20 articles. Her published works are related to the analysis of errors in spatial databases and geomatics applied to cultural heritage.

Laura Fragoso-Campón was born in 1978 in Cádiz, Spain. She received the Technical degree in civil engineering from the University of Extremadura, Badajoz, Spain, in 1999, and the master's degree in civil engineering (Ingeniera de Caminos, Canales y Puertos) from the Polytechnic University of Madrid, Madrid, Spain, in 2003. She is currently working toward the Ph.D. degree in remote sensing and hydrology with the Polytechnic School, University of Extremadura.

She is the author of five articles, and her published works are related to remote sensing and hydrology.

Prof. Campón is a member of the Spanish Society of Remote Sensing.